

Study of the $e^+e^- \to Z\gamma$ process at LEP and limits on triple neutral-gauge-boson couplings

P. Achard, O. Adriani, M. Aguilar-Benitez, J. Alcaraz, G. Alemanni, J. Allaby, A. Aloisio, M.G. Alviggi, H. Anderhub, V.P. Andreev, et al.

▶ **To cite this version:**

P. Achard, O. Adriani, M. Aguilar-Benitez, J. Alcaraz, G. Alemanni, et al.. Study of the $e^+e^- \to Z\gamma$ process at LEP and limits on triple neutral-gauge-boson couplings. Physics Letters B, 2004, 597, pp.119-130. 10.1016/j.physletb.2004.07.002 . in2p3-00022195

HAL Id: in2p3-00022195
https://hal.in2p3.fr/in2p3-00022195

Submitted on 2 Sep 2004

HAL is a multi-disciplinary open access archive for the deposit and dissemination of scientific research documents, whether they are published or not. The documents may come from teaching and research institutions in France or abroad, or from public or private research centers.

L'archive ouverte pluridisciplinaire **HAL**, est destinée au dépôt et à la diffusion de documents scientifiques de niveau recherche, publiés ou non, émanant des établissements d'enseignement et de recherche français ou étrangers, des laboratoires publics ou privés.

arXiv:hep-ex/0407012 v1 6 Jul 2004

EUROPEAN ORGANIZATION FOR NUCLEAR RESEARCH

CERN-PH-EP/2004-014
April 19, 2004

Study of the $e^+e^- \to Z\gamma$ Process at LEP and Limits on Triple Neutral-Gauge-Boson Couplings

The L3 Collaboration

Abstract

The process $e^+e^- \to Z\gamma$, where the Z boson decays into hadrons or neutrinos, is studied with data collected with the L3 detector at LEP at centre-of-mass energies from 189 GeV up to 209 GeV. The cross sections are measured and found to be in agreement with the Standard Model predictions. Limits on triple neutral-gauge-boson couplings, forbidden in the Standard Model at tree level, are derived. Limits on the energy scales at which the anomalous couplings could be manifest are set. They range from 0.3 TeV to 2.3 TeV depending on the new physics effect under consideration.

Submitted to *Phys. Lett. B*

1 Introduction

The process $e^+e^- \to Z\gamma$ allows to test the existence of new physics [1], such as anomalous couplings between neutral gauge bosons. Effects coming from $ZZ\gamma$ and $Z\gamma\gamma$ couplings are expected to be very small in the Standard Model [1, 2], but can be enhanced in compositeness models [3] or if new particles enter in higher order corrections. Anomalous $ZZ\gamma$ and $Z\gamma\gamma$ couplings would increase the $e^+e^- \to Z\gamma$ cross section and produce an enhancement of large polar angle photons.

Assuming only Lorentz and $U(1)_{em}$ gauge invariance, the most general form of the $ZV\gamma$ vertices, with a real Z and γ in the final state, is parametrized by means of the anomalous couplings, h_i^V $(i = 1 \ldots 4; V = \gamma, Z)$ [4]. The couplings h_1^V and h_2^V are CP violating whereas h_3^V and h_4^V are CP conserving. All these couplings are zero at tree level in the Standard Model, and only the CP conserving ones are non-vanishing ($\sim 10^{-4}$) at the one-loop level [1, 2]. An alternative parametrization, which introduces the energy scales of new physics, Λ_{iV}, is [5]:

$$\frac{\sqrt{\alpha}\, h_i^V}{m_Z^2} \equiv \frac{1}{\Lambda_{iV}^2} \quad i = 1, 3 \tag{1}$$

$$\frac{\sqrt{\alpha}\, h_i^V}{m_Z^4} \equiv \frac{1}{\Lambda_{iV}^4} \quad i = 2, 4, \tag{2}$$

where α is the fine-structure constant. The fact that there are always two identical particles at the vertex forbids the three bosons to be on-shell. This means the $ZZ\gamma$ and $Z\gamma\gamma$ vertices may only appear if one of the bosons is off-shell. A treatment of these vertices where all three bosons are off-shell is discussed in Reference 6. In this Letter, the $e^+e^- \to Z\gamma$ process is analyzed. The maximal experimental sensitivity is achieved with the analysis of the $e^+e^- \to f\bar{f}\gamma$ process, with the fermion pair in the vicinity of the Z resonance, where the signal statistics is high and backgrounds are reduced. In this scenario, effects from an off-shell final-state Z boson are negligible [7].

L3 published results [8] on the $e^+e^- \to Z\gamma$ process, setting limits on $ZZ\gamma$ and $Z\gamma\gamma$ couplings from data obtained at lower center-of-mass energies (161 GeV $\leq \sqrt{s} \leq$ 189 GeV). Results have also been published by other experiments at LEP [9] and at the TEVATRON [10]. In this Letter we present results for the highest energies collected at LEP.

The phase space definition for the $e^+e^- \to Z\gamma$ process requires a photon with energy greater than 20 GeV and polar angle in the range $5^\circ < \theta_\gamma < 175^\circ$. Every cross section and acceptance in this Letter is referred to this fiducial region .

2 Data and Monte Carlo Samples

Data collected by the L3 detector [11] at $\sqrt{s} = 189$ GeV $-$ 209 GeV with a total luminosity of about 626pb^{-1} are used to study the $e^+e^- \to Z\gamma$ process in the channels $e^+e^- \to q\bar{q}\gamma$ and $e^+e^- \to \nu\bar{\nu}\gamma$.

The Standard Model processes giving rise to these final states are modelled with KK2f, for $e^+e^- \to q\bar{q}\gamma(\gamma)$, and KKMC, for $e^+e^- \to \nu\bar{\nu}\gamma(\gamma)$ [12]. Both programs are general purpose Monte Carlo generators for the process $e^+e^- \to f\bar{f} + n\gamma$, containing complete $O(\alpha^2)$ corrections from initial- and final-state radiation, including their interference. Data for $e^+e^- \to \nu\bar{\nu}\gamma(\gamma)$ at $\sqrt{s} = 189$ GeV, previously analysed and compared to the KORALZ Monte Carlo [13], are now re-analysed using KKMC.

Background processes are simulated with EXCALIBUR [14] for the four-fermion final states, PHOJET [15] and DIAG36 [16] for two-photon collisions with hadrons or leptons in the final state, respectively, and BHWIDE [17] and TEEGG [18] for $e^+e^- \to e^+e^-\gamma(\gamma)$.

All generated events are passed through a simulation of the L3 detector [19] and the same analysis procedure as used for the data. Time-dependent detector inefficiencies, monitored during data-taking, are also taken into account.

3 Event Selection

3.1 Photon Selection

The main signature of the process $e^+e^- \to Z\gamma$ is the production of a high energy photon. A photon candidate is identified as a shower in the barrel or endcap region of the BGO crystal electromagnetic calorimeter, consistent with an electromagnetic shower and with a minimum energy of 5 GeV. The mass of the system recoiling against the photon of energy E_γ: $m_{rec} = (s - 2E_\gamma\sqrt{s})^{1/2}$, is required to satisfy 80 GeV $< m_{rec} <$ 110 GeV, consistent with Z-boson production. For the $\sqrt{s}$ values considered, the cuts on the recoiling mass correspond to photon energies between 62 GeV and 89 GeV.

3.2 Selection of $e^+e^- \to q\bar{q}\gamma$ Events

In addition to requiring a photon candidate, $e^+e^- \to q\bar{q}\gamma$ events are selected by demanding that:

- the event have more than 6 charged tracks reconstructed in the fiducial volume of the tracking chamber and more than 11 calorimetric clusters in the electromagnetic calorimeter.
- the transverse energy imbalance be less than 15% of the total reconstructed energy and the longitudinal energy imbalance less than 20% of the same quantity.
- the angle of the photon candidate with respect to the beam direction, θ_γ, satisfy $|\cos\theta_\gamma| < 0.97$.

In order to reject electrons produced in the central region, photon candidates with $|\cos\theta_\gamma| < 0.90$ are not considered if they are associated to a charged track in the central tracking chamber. This requirement eliminates a substantial contamination of background processes. For the last period of data taking, corresponding to data at $\sqrt{s} > 202$ GeV, this rejection cut is relaxed to $|\cos\theta_\gamma| < 0.85$ to account for different running conditions of the detector. This change increases the contamination from background processes.

Table 1 lists the data luminosity analysed at each $\sqrt{s}$, the selection efficiency, the background level and the number of selected events, after background subtraction.

The trigger inefficiency is estimated to be negligible due to the redundancy of subtriggers involved in tagging this final state. Two backgrounds contribute in equal proportions: the $e^+e^- \to q\bar{q}'e\nu$ and $e^+e^- \to q\bar{q}e^+e^-$ processes, where one electron fakes a photon.

Figure 1 shows the distributions of m_{rec}, $\cos\theta_\gamma$ and the invariant mass of the hadron system, reconstructed from jet and photon directions and $\sqrt{s}$.

The resolution of the L3 electromagnetic calorimeter, better than 1%, allows the observation of a tail in Figure 1a, for m_{rec} above the nominal Z mass, due to initial state radiation photons.

3.3 Selection of $e^+e^- \to \nu\bar{\nu}\gamma$ Events

In addition to the presence of a photon, selected as described above, the events from the $e^+e^- \to \nu\bar{\nu}\gamma$ process are selected by the following criteria:

- the event must have at most 5 calorimetric clusters, due to low energy (< 1 GeV) initial state photons or noise in the calorimeter. The number of hits in the tracking chamber associated to a calorimetric cluster, including the photon candidate, must not exceed 40% of the expected number of hits for a charged track.
- the angle of the photon candidate with respect to the beam direction must satisfy $|\cos\theta_\gamma| < 0.96$. This range differs from that of the hadronic channel in order to match the angular coverage of the central tracking chamber used to reject electrons.
- the total reconstructed energy, E_{tot}, must fulfill $\sqrt{s} - E_{tot} > 0.95\,E_{tot}$ and the transverse energy imbalance must be greater than $0.2E_{tot}$.
- To suppress cosmic ray background, there must be at least one scintillator time measurement within ± 5 ns of the beam crossing time. The scintillator signals must be associated with calorimetric clusters.

The background in the selected sample is found to be negligible. Table 2 lists the data luminosity analysed at each $\sqrt{s}$ and the selection efficiency. The selection efficiency includes trigger efficiency, evaluated to be around 95% by using two independent data samples from the $e^+e^- \to e^+e^-$ and $e^+e^- \to \gamma\gamma$ processes. The number of selected events is also given. Figure 2 shows the distributions of m_{rec} and $\cos\theta_\gamma$.

4 Cross Section Measurements

The measured cross sections for both the $e^+e^- \to q\bar{q}\gamma$ and $e^+e^- \to \nu\bar{\nu}\gamma$ processes are presented in Tables 1 and 2, respectively, together with Standard Model predictions. Good agreement is observed. The uncertainty on the expected cross section, σ_{SM}, takes into account a 1% theory uncertainty of KK2f and KKMC and the finite Monte Carlo statistics generated for these studies.

In addition to cross sections, in Table 3 we present more detailed information for the $e^+e^- \to q\bar{q}\gamma$ process on the number of events observed and expected, the background and selection efficiencies, in bins of m_{rec} and $|\cos\theta_\gamma|$. Similar tables are given elsewhere [20] for the $e^+e^- \to \nu\bar{\nu}\gamma$ process.

The main sources of systematic uncertainties are summarized in Table 4. The largest contribution is due to the selection procedure. A change of 3% in the values of the cut on m_{rec} corresponds to 0.8% and 1.5% uncertainties for hadronic and invisible decay modes, respectively. Changes in the photon energy scale give uncertainties of 0.4% and 0.6% for the hadronic and invisible channels, respectively. The uncertainty from limited Monte Carlo statistics amounts to 0.4% for the $e^+e^- \to \nu\bar{\nu}\gamma$ channel and varies between 0.1% and 0.4% for the $e^+e^- \to q\bar{q}\gamma$ channel. The accuracy on the luminosity estimation gives a 0.2% uncertainty. Uncertainty in the measurement of the trigger efficiency contributes an additional 0.3% in the $e^+e^- \to \nu\bar{\nu}\gamma$ process. A variation of 10% in the background level corresponds to a 0.3% uncertainty in the hadronic channel.

The variation of the sum of the $e^+e^- \to q\bar{q}\gamma$ and $e^+e^- \to \nu\bar{\nu}\gamma$ cross sections with $\sqrt{s}$ is presented in Figure 3. Cross sections at $\sqrt{s} = 161, 172$ and 183 GeV, already published by L3 [8], are included for completeness. The relative deviation from the Standard Model predictions as a function of $\sqrt{s}$ is also shown. Good agreement is found.

5 Triple Neutral-Gauge-Boson Couplings

Since deviations from Standard Model expectations are found neither for the $e^+e^- \to q\bar{q}\gamma$ nor for the $e^+e^- \to \nu\bar{\nu}\gamma$ process, limits on anomalous triple-neutral-gauge boson couplings are extracted by using an optimal observable method [21].

5.1 Optimal Observable Method

In the presence of anomalous couplings, the cross section for the process $e^+e^- \to Z\gamma$ is proportional to $|M_{SM} + M_{AC}|^2$, with M_{SM} and $M_{AC}(h_i^V)$ the Standard Model and anomalous coupling amplitudes, respectively.

As M_{AC} depends linearly on the h_i^V (i=1 ... 4; V=γ, Z) parameters, the differential cross section can be written as a quadratic function on the anomalous couplings:

$$\frac{d\sigma}{d\vec{\Omega}} = c_0(\vec{\Omega}) + \sum_{i=1}^{4} \sum_{V=\gamma,\mathrm{Z}} c_{1,i,V}(\vec{\Omega}) h_i^V + \sum_{i=1}^{4} \sum_{V=\gamma,\mathrm{Z}} \sum_{j=1}^{4} \sum_{V'=\gamma,\mathrm{Z}} c_{2,ij,V,V'}(\vec{\Omega}) h_i^V h_j^{V'} \tag{3}$$

where $\vec{\Omega}$ stands for the phase space variables defining the final state, $c_0(\vec{\Omega})$ is the Standard Model cross section and $c_{1,i,V}$ and $c_{2,ij,V,V'}$ are coefficients related to the anomalous amplitudes.

The variables defined for each coupling as:

$$\mathcal{O}_{1,i,V}(\vec{\Omega}) \equiv \frac{c_{1,i,V}(\vec{\Omega})}{c_0(\vec{\Omega})} \tag{4}$$

$$\mathcal{O}_{2,ij,V,V'}(\vec{\Omega}) \equiv \frac{c_{2,ij,V,V'}(\vec{\Omega})}{c_0(\vec{\Omega})} \tag{5}$$

are called "optimal variables" as they contain the full kinematic information on the event and allow the determination of the parameters h_i^V with the maximum possible statistical precision. If the parameters h_i^V are sufficiently small, the quadratic term can be neglected and all the information in the multidimensional phase space $\vec{\Omega}$ is projected into the variable $\mathcal{O}_1$.

In order to extract the h_i^V's, a binned maximum-likelihood fit of the expected distribution of the optimal variable $\mathcal{O}_{1,i,V}$ is performed to the data, assuming a Poisson density distribution in each bin. Both the shape of the optimal variable distribution, which includes energy and angular information, and the total number of events contribute to the fit. The expected number of events in the presence of anomalous couplings is computed from a Standard Model reference sample by applying a reweighting technique, in which each Monte Carlo event is weighted with the following quantity, defined at the generator level:

$$W(h_i^V) = \frac{|M_{SM} + M_{AC}(h_i^V)|^2}{|M_{SM}|^2} \tag{6}$$

The comparison between expected and observed events is done at the level of reconstructed variables so that all experimental effects, such as detector resolution or selection efficiencies, are automatically taken into account.

5.2 Limits on Anomalous Couplings

Making use of the optimal observable method and taking into consideration the information on the total event rate for each process and the phase space variables defining the final state, limits at 95% Confidence Level (CL) are set on the h_i^V couplings. The reconstructed set of variables used to compute the optimal variables is $\vec{\Omega} = (E_\gamma, \theta_\gamma, \phi_\gamma, \theta_f^{\mathrm{Z}}, \phi_f^{\mathrm{Z}})$, where E_γ, θ_γ and ϕ_γ are the energy and angles of the photon, and θ_f^{Z} and ϕ_f^{Z} the angles of the fermion f in the Z rest frame. In the $\mathrm{e^+e^-} \to \nu\bar{\nu}\gamma$ channel only the three photon variables are used.

Distributions of the optimal variables for the couplings h_1^{Z} and h_4^{γ} are shown in Figure 4. The regions of maximal sensitivity to the existence of anomalous couplings correspond to the largest absolute values of the optimal variables, where discrepancies with Standard Model predictions are expected to be larger.

The 95% CL limits on each individual anomalous coupling, combining both channels and from all data collected at 189 GeV $\leq \sqrt{s} \leq$ 209 GeV, are obtained from one-dimensional fits. The results are given in Table 5 and they correspond to the following intervals:

$$
\begin{array}{ll}
-0.153 < h_1^{\mathrm{Z}} < 0.141 & -0.057 < h_1^{\gamma} < 0.057 \\
-0.087 < h_2^{\mathrm{Z}} < 0.079 & -0.050 < h_2^{\gamma} < 0.023 \\
-0.220 < h_3^{\mathrm{Z}} < 0.112 & -0.059 < h_3^{\gamma} < 0.004 \\
-0.068 < h_4^{\mathrm{Z}} < 0.148 & -0.004 < h_4^{\gamma} < 0.042
\end{array}
$$

To obtain these intervals one parameter is left free at a time, setting the other seven anomalous couplings to zero. These limits supersede the previous L3 results, obtained with a smaller data sample at lower centre-of-mass energies [8]. The observed limits agree within 10% with the expected limits.

Limits coming from even couplings, h_2^V and h_4^V are more stringent than those coming from odd couplings, h_1^V and h_3^V, as the former correspond to operators of dimension eight, while the latter correspond to dimension six operators [1, 2], as reflected in equations (1) and (2) in the different dependence of the parameters on the mass m_{Z} and the energy scales. These relations imply that the Standard Model is tested more stringently in the linear expansion of the effective Lagrangian when considering the even couplings.

Fits to the two-dimensional distributions of the optimal observables are performed to determine the pairs of CP-violating (h_1^V, h_2^V) and CP-conserving couplings (h_3^V, h_4^V), keeping in each case the other couplings fixed at zero. Results at 95% CL are shown in Table 6. A strong correlation between the two CP-violating or CP-conserving parameters is observed. Contours for the 68% and 95% CL two-dimensional limits on each pair of couplings are shown in Figure 5. The main sources of systematic uncertainties, discussed in section 4, are included in the limits calculation. They contribute 0.02 to one-dimensional limits and 0.03 for two-dimensional limits.

If the data are interpreted in terms of new physics scales using formulae (1) and (2), lower limits at 95% CL on the scale of new physics are obtained as:

$$\begin{array}{ll} \Lambda_{1Z} > 0.8 \text{ TeV} & \Lambda_{1\gamma} > 1.3 \text{ TeV} \\ \Lambda_{2Z} > 0.3 \text{ TeV} & \Lambda_{2\gamma} > 0.4 \text{ TeV} \\ \Lambda_{3Z} > 0.8 \text{ TeV} & \Lambda_{3\gamma} > 2.3 \text{ TeV} \\ \Lambda_{4Z} > 0.3 \text{ TeV} & \Lambda_{4\gamma} > 0.4 \text{ TeV}. \end{array}$$

To determine the confidence levels the probability distributions are normalized over the physical range of the parameters, $\Lambda > 0$.

6 Conclusions

The analysis of the process $e^+e^- \to Z\gamma$ in the final states $Z\gamma \to q\bar{q}\gamma$ and $Z\gamma \to \nu\bar{\nu}\gamma$ with 620 pb^{-1} of luminosity collected by the L3 detector at $189 \leq \sqrt{s} \leq 209$ GeV reveals a very good agreement between the measured cross sections and the Standard Model prediction. Detailed information on the hadronic final-state events are given in form of tables to allow constraints of future models.

These measurements establish upper limits at 95 % CL on the values of anomalous couplings, h_i^V, appearing in the triple neutral-gauge-boson vertices, ZZγ and Z$\gamma\gamma$. At tree level in the Standard Model these couplings are zero. We observe no deviation from this prediction and constrain possible values of the anomalous couplings in intervals of widths between 0.05 and 0.33, depending on the coupling considered. These limits improve and supersede our previous limits [8].

References

[1] F.M. Renard, Nucl. Phys. **B 196** (1982) 93.

[2] A. Barroso *et al.*, Z. Phys. **C 28** (1985) 149.

[3] F.M. Renard, Phys. Lett. **B 126** (1983) 59;
M. Claudson, E. Farhi, R.L. Jaffe, Phys. Rev. **D 34** (1986) 873.

[4] K. Hagiwara, R.D. Peccei, D. Zeppenfeld and K. Hikasa, Nucl. Phys. **B282** (1987) 253;
G. J. Gounaris, J. Layssac and F. M. Renard, Phys. Rev. **D 61** (2000) 073013.

[5] P. Mery, M. Perrottet, F.M. Renard, Z. Phys. **C 38** (1988) 579.

[6] G. J. Gounaris, J. Layssac and F. M. Renard, Phys. Rev. **D 62** (2000) 073012.

[7] J. Alcaraz, Phys. Rev. **D 65** (2002) 075020.

[8] L3 Collab., M. Acciarri *et al.*, Phys. Lett. **B 436** (1998) 187;
L3 Collab., M. Acciarri *et al.*, Phys. Lett. **B 489** (2000) 55.

[9] DELPHI Collab., P. Abreu *et al.*, Phys. Lett. **B 423** (1998) 194;
OPAL Collab., G. Abbiendi *et al.*, Eur. Phys. J. **C 17** (2000) 553.

[10] CDF Collab., F. Abe *et al.*, Phys. Rev. Lett. **74** (1995) 1941;
D0 Collab., S. Abachi *et al.*, Phys. Rev. Lett. **78** (1997) 3640;
D0 Collab., B. Abbott *et al.*, Phys. Rev. **D 57** (1998) 3817.

[11] L3 Collab., B. Adeva *et al.*, Nucl. Inst. and Meth. **A289** (1990) 35;
L3 Collab., O. Adriani *et al.*, Phys. Rep. **236** (1993) 1;
M. Chemarin *et al.*, Nucl. Inst. and Meth. **A349** (1994) 345;
M. Acciarri *et al.*, Nucl. Inst. and Meth. **A351** (1994) 300;
G. Basti *et al.*, Nucl. Inst. and Meth. **A374** (1996) 293;
I.C. Brock *et al.*, Nucl. Inst. and Meth. **A381** (1996) 236;
A. Adam *et al.*, Nucl. Inst. and Meth. **A383** (1996) 342.

[12] KK2f version 4.12 is used for $e^+e^- \to q\bar{q}\gamma$ and version 4.19 for $e^+e^- \to \nu\bar{\nu}\gamma$:
S. Jadach, B.F.L. Ward and Z. Was, Comput. Phys. Commun. **130** (2000) 260;
S. Jadach, B.F.L. Ward and Z. Was, Phys. Rev. **D 63** (2001) 113009;
D. Bardin, S. Jadach, T. Riemann and Z. Was, Eur. Phys. J. **C 24** (2002) 373.

[13] KORALZ version 4.04 is used:
S. Jadach, B.F.L. Ward and Z. Wąs, Comp. Phys. Comm. **79** (1994) 503.

[14] EXCALIBUR version 1.11 is used:
F.A. Berends, R. Kleiss and R. Pittau, Comp. Phys. Comm. **85** (1995) 437.

[15] PHOJET version 1.05 is used:
R. Engel, Z. Phys. **C 66** (1995) 203;
R. Engel and J. Ranft, Phys. Rev. **D 54** (1996) 4244.

[16] DIAG36 Monte Carlo:
F.A. Berends, P.H. Daverfelt and R. Kleiss, Nucl. Phys. **B 253** (1985) 441;
F.A. Berends, P.H. Daverfelt and R. Kleiss, Comp. Phys. Comm. **40** (1986) 285.

[17] BHWIDE version 1.03 is used:
S. Jadach, W. Placzek and B.F.L. Ward, Phys. Lett. **B 390** (1997) 298.

[18] TEEGG version 7.1 is used:
D. Karlen, Nucl. Phys. **B 289** (1987) 23.

[19] The L3 detector simulation is based on GEANT Version 3.15:
R. Brun *et al.*, preprint CERN–DD/EE/84–1 (1984), revised 1987.
The GHEISHA program (H. Fesefeldt, RWTH Aachen Report PITHA 85/02 (1985))
is used to simulate hadronic interactions.

[20] L3 Collab., P. Achard *et al.*, Phys. Lett. **B 587** (2004) 16.

[21] G.K. Fanourakis, D. Fassouliotis and S.E. Tzamarias, Nucl. Instr. Meth. **A 414** (1998) 399;
M. Diehl and O. Nachtmann, Z. Phys. **C 62** (1994) 397; Eur. Phys. J. **C 1** (1998) 177.

The L3 Collaboration:

P.Achard,[20] O.Adriani,[17] M.Aguilar-Benitez,[25] J.Alcaraz,[25] G.Alemanni,[23] J.Allaby,[18] A.Aloisio,[29] M.G.Alviggi,[29] H.Anderhub,[49] V.P.Andreev,[6,34] F.Anselmo,[8] A.Arefiev,[28] T.Azemoon,[3] T.Aziz,[9] P.Bagnaia,[39] A.Bajo,[25] G.Baksay,[26] L.Baksay,[26] S.V.Baldew,[2] S.Banerjee,[9] Sw.Banerjee,[4] A.Barczyk,[49,47] R.Barillère,[18] P.Bartalini,[23] M.Basile,[8] N.Batalova,[46] R.Battiston,[33] A.Bay,[23] F.Becattini,[17] U.Becker,[13] F.Behner,[49] L.Bellucci,[17] R.Berbeco,[3] J.Berdugo,[25] P.Berges,[13] B.Bertucci,[33] B.L.Betev,[49] M.Biasini,[33] M.Biglietti,[29] A.Biland,[49] J.J.Blaising,[4] S.C.Blyth,[35] G.J.Bobbink,[2] A.Böhm,[1] L.Boldizsar,[12] B.Borgia,[39] S.Bottai,[17] D.Bourilkov,[49] M.Bourquin,[20] S.Braccini,[20] J.G.Branson,[41] F.Brochu,[4] J.D.Burger,[13] W.J.Burger,[33] X.D.Cai,[13] M.Capell,[13] G.Cara Romeo,[8] G.Carlino,[29] A.Cartacci,[17] J.Casaus,[25] F.Cavallari,[39] N.Cavallo,[36] C.Cecchi,[33] M.Cerrada,[25] M.Chamizo,[20] Y.H.Chang,[44] M.Chemarin,[24] A.Chen,[44] G.Chen,[7] G.M.Chen,[7] H.F.Chen,[22] H.S.Chen,[7] G.Chiefari,[29] L.Cifarelli,[40] F.Cindolo,[8] I.Clare,[13] R.Clare,[38] G.Coignet,[4] N.Colino,[25] S.Costantini,[39] B.de la Cruz,[25] S.Cucciarelli,[33] J.A.van Dalen,[31] R.de Asmundis,[29] P.Déglon,[20] J.Debreczeni,[12] A.Degré,[4] K.Dehmelt,[26] K.Deiters,[47] D.della Volpe,[29] E.Delmeire,[20] P.Denes,[37] F.DeNotaristefani,[39] A.De Salvo,[49] M.Diemoz,[39] M.Dierckxsens,[2] C.Dionisi,[39] M.Dittmar,[49] A.Doria,[29] M.T.Dova,[10,♯] D.Duchesneau,[4] M.Duda,[1] B.Echenard,[20] A.Eline,[18] A.El Hage,[1] H.El Mamouni,[24] A.Engler,[35] F.J.Eppling,[13] P.Extermann,[20] M.A.Falagan,[25] S.Falciano,[39] A.Favara,[32] J.Fay,[24] O.Fedin,[34] M.Felcini,[49] T.Ferguson,[35] H.Fesefeldt,[1] E.Fiandrini,[33] J.H.Field,[20] F.Filthaut,[31] P.H.Fisher,[13] W.Fisher,[37] I.Fisk,[41] G.Forconi,[13] K.Freudenreich,[49] C.Furetta,[27] Yu.Galaktionov,[28,13] S.N.Ganguli,[9] P.Garcia-Abia,[25] M.Gataullin,[32] S.Gentile,[39] S.Giagu,[39] Z.F.Gong,[22] G.Grenier,[24] O.Grimm,[49] M.W.Gruenewald,[16] M.Guida,[40] R.van Gulik,[2] V.K.Gupta,[37] A.Gurtu,[9] L.J.Gutay,[46] D.Haas,[5] D.Hatzifotiadou,[8] T.Hebbeker,[1] A.Hervé,[18] J.Hirschfelder,[35] H.Hofer,[49] M.Hohlmann,[26] G.Holzner,[49] S.R.Hou,[44] Y.Hu,[31] B.N.Jin,[7] L.W.Jones,[3] P.de Jong,[2] I.Josa-Mutuberría,[25] M.Kaur,[14] M.N.Kienzle-Focacci,[20] J.K.Kim,[43] J.Kirkby,[18] W.Kittel,[31] A.Klimentov,[13,28] A.C.König,[31] M.Kopal,[46] V.Koutsenko,[13,28] M.Kräber,[49] R.W.Kraemer,[35] A.Krüger,[48] A.Kunin,[13] P.Ladron de Guevara,[25] I.Laktineh,[24] G.Landi,[17] M.Lebeau,[18] A.Lebedev,[13] P.Lebrun,[24] P.Lecomte,[49] P.Lecoq,[18] P.Le Coultre,[49] J.M.Le Goff,[18] R.Leiste,[48] M.Levtchenko,[27] P.Levtchenko,[34] C.Li,[22] S.Likhoded,[48] C.H.Lin,[44] W.T.Lin,[44] F.L.Linde,[2] L.Lista,[29] Z.A.Liu,[7] W.Lohmann,[48] E.Longo,[39] Y.S.Lu,[7] C.Luci,[39] L.Luminari,[39] W.Lustermann,[49] W.G.Ma,[22] L.Malgeri,[20] A.Malinin,[28] C.Maña,[25] J.Mans,[37] J.P.Martin,[24] F.Marzano,[39] K.Mazumdar,[9] R.R.McNeil,[6] S.Mele,[18,29] L.Merola,[29] M.Meschini,[17] W.J.Metzger,[31] A.Mihul,[11] H.Milcent,[18] G.Mirabelli,[39] J.Mnich,[1] G.B.Mohanty,[9] G.S.Muanza,[24] A.J.M.Muijs,[2] B.Musicar,[41] M.Musy,[39] S.Nagy,[15] S.Natale,[20] M.Napolitano,[29] F.Nessi-Tedaldi,[49] H.Newman,[32] A.Nisati,[39] T.Novak,[31] H.Nowak,[48] R.Ofierzynski,[49] G.Organtini,[39] I.Pal,[46] C.Palomares,[25] P.Paolucci,[29] R.Paramatti,[39] G.Passaleva,[17] S.Patricelli,[29] T.Paul,[10] M.Pauluzzi,[33] C.Paus,[13] F.Pauss,[49] M.Pedace,[39] S.Pensotti,[27] D.Perret-Gallix,[4] B.Petersen,[31] D.Piccolo,[29] F.Pierella,[8] M.Pioppi,[33] P.A.Piroué,[37] E.Pistolesi,[27] V.Plyaskin,[28] M.Pohl,[20] V.Pojidaev,[17] J.Pothier,[18] D.Prokofiev,[34] J.Quartieri,[40] G.Rahal-Callot,[49] M.A.Rahaman,[9] P.Raics,[15] N.Raja,[9] R.Ramelli,[49] P.G.Rancoita,[27] R.Ranieri,[17] A.Raspereza,[48] P.Razis,[30] D.Ren,[49] M.Rescigno,[39] S.Reucroft,[10] S.Riemann,[48] K.Riles,[3] B.P.Roe,[3] L.Romero,[25] A.Rosca,[48] C.Rosemann,[1] C.Rosenbleck,[1] S.Rosier-Lees,[4] S.Roth,[1] J.A.Rubio,[18] G.Ruggiero,[17] H.Rykaczewski,[49] A.Sakharov,[49] S.Saremi,[6] S.Sarkar,[39] J.Salicio,[18] E.Sanchez,[25] C.Schäfer,[18] V.Schegelsky,[34] H.Schopper,[21] D.J.Schotanus,[31] C.Sciacca,[29] L.Servoli,[33] S.Shevchenko,[32] N.Shivarov,[42] V.Shoutko,[13] E.Shumilov,[28] A.Shvorob,[32] D.Son,[43] C.Souga,[24] P.Spillantini,[17] M.Steuer,[13] D.P.Stickland,[37] B.Stoyanov,[42] A.Straessner,[20] K.Sudhakar,[9] G.Sultanov,[42] L.Z.Sun,[22] S.Sushkov,[1] H.Suter,[49] J.D.Swain,[10] Z.Szillasi,[26,¶] X.W.Tang,[7] P.Tarjan,[15] L.Tauscher,[5] L.Taylor,[10] B.Tellili,[24] D.Teyssier,[24] C.Timmermans,[31] Samuel C.C.Ting,[13] S.M.Ting,[13] S.C.Tonwar,[9] J.Tóth,[12] C.Tully,[37] K.L.Tung,[7] J.Ulbricht,[49] E.Valente,[39] R.T.Van de Walle,[31] R.Vasquez,[46] V.Veszpremi,[26] G.Vesztergombi,[12] I.Vetlitsky,[28] D.Vicinanza,[40] G.Viertel,[49] S.Villa,[38] M.Vivargent,[4] S.Vlachos,[5] I.Vodopianov,[26] H.Vogel,[35] H.Vogt,[48] I.Vorobiev,[35,28] A.A.Vorobyov,[34] M.Wadhwa,[5] Q.Wang,[31] X.L.Wang,[22] Z.M.Wang,[22] M.Weber,[18] H.Wilkens,[31] S.Wynhoff,[37] L.Xia,[32] Z.Z.Xu,[22] J.Yamamoto,[3] B.Z.Yang,[22] C.G.Yang,[7] H.J.Yang,[3] M.Yang,[7] S.C.Yeh,[45] An.Zalite,[34] Yu.Zalite,[34] Z.P.Zhang,[22] J.Zhao,[22] G.Y.Zhu,[7] R.Y.Zhu,[32] H.L.Zhuang,[7] A.Zichichi,[8,18,19] B.Zimmermann,[49] M.Zöller.[1]

1 III. Physikalisches Institut, RWTH, D-52056 Aachen, Germany[§]
2 National Institute for High Energy Physics, NIKHEF, and University of Amsterdam, NL-1009 DB Amsterdam, The Netherlands
3 University of Michigan, Ann Arbor, MI 48109, USA
4 Laboratoire d'Annecy-le-Vieux de Physique des Particules, LAPP,IN2P3-CNRS, BP 110, F-74941 Annecy-le-Vieux CEDEX, France
5 Institute of Physics, University of Basel, CH-4056 Basel, Switzerland
6 Louisiana State University, Baton Rouge, LA 70803, USA
7 Institute of High Energy Physics, IHEP, 100039 Beijing, China[△]
8 University of Bologna and INFN-Sezione di Bologna, I-40126 Bologna, Italy
9 Tata Institute of Fundamental Research, Mumbai (Bombay) 400 005, India
10 Northeastern University, Boston, MA 02115, USA
11 Institute of Atomic Physics and University of Bucharest, R-76900 Bucharest, Romania
12 Central Research Institute for Physics of the Hungarian Academy of Sciences, H-1525 Budapest 114, Hungary[‡]
13 Massachusetts Institute of Technology, Cambridge, MA 02139, USA
14 Panjab University, Chandigarh 160 014, India
15 KLTE-ATOMKI, H-4010 Debrecen, Hungary[¶]
16 Department of Experimental Physics, University College Dublin, Belfield, Dublin 4, Ireland
17 INFN Sezione di Firenze and University of Florence, I-50125 Florence, Italy
18 European Laboratory for Particle Physics, CERN, CH-1211 Geneva 23, Switzerland
19 World Laboratory, FBLJA Project, CH-1211 Geneva 23, Switzerland
20 University of Geneva, CH-1211 Geneva 4, Switzerland
21 University of Hamburg, D-22761 Hamburg, Germany
22 Chinese University of Science and Technology, USTC, Hefei, Anhui 230 029, China[△]
23 University of Lausanne, CH-1015 Lausanne, Switzerland
24 Institut de Physique Nucléaire de Lyon, IN2P3-CNRS,Université Claude Bernard, F-69622 Villeurbanne, France
25 Centro de Investigaciones Energéticas, Medioambientales y Tecnológicas, CIEMAT, E-28040 Madrid, Spain[♭]
26 Florida Institute of Technology, Melbourne, FL 32901, USA
27 INFN-Sezione di Milano, I-20133 Milan, Italy
28 Institute of Theoretical and Experimental Physics, ITEP, Moscow, Russia
29 INFN-Sezione di Napoli and University of Naples, I-80125 Naples, Italy
30 Department of Physics, University of Cyprus, Nicosia, Cyprus
31 University of Nijmegen and NIKHEF, NL-6525 ED Nijmegen, The Netherlands
32 California Institute of Technology, Pasadena, CA 91125, USA
33 INFN-Sezione di Perugia and Università Degli Studi di Perugia, I-06100 Perugia, Italy
34 Nuclear Physics Institute, St. Petersburg, Russia
35 Carnegie Mellon University, Pittsburgh, PA 15213, USA
36 INFN-Sezione di Napoli and University of Potenza, I-85100 Potenza, Italy
37 Princeton University, Princeton, NJ 08544, USA
38 University of Californa, Riverside, CA 92521, USA
39 INFN-Sezione di Roma and University of Rome, "La Sapienza", I-00185 Rome, Italy
40 University and INFN, Salerno, I-84100 Salerno, Italy
41 University of California, San Diego, CA 92093, USA
42 Bulgarian Academy of Sciences, Central Lab. of Mechatronics and Instrumentation, BU-1113 Sofia, Bulgaria
43 The Center for High Energy Physics, Kyungpook National University, 702-701 Taegu, Republic of Korea
44 National Central University, Chung-Li, Taiwan, China
45 Department of Physics, National Tsing Hua University, Taiwan, China
46 Purdue University, West Lafayette, IN 47907, USA
47 Paul Scherrer Institut, PSI, CH-5232 Villigen, Switzerland
48 DESY, D-15738 Zeuthen, Germany
49 Eidgenössische Technische Hochschule, ETH Zürich, CH-8093 Zürich, Switzerland
§ Supported by the German Bundesministerium für Bildung, Wissenschaft, Forschung und Technologie.
‡ Supported by the Hungarian OTKA fund under contract numbers T019181, F023259 and T037350.
¶ Also supported by the Hungarian OTKA fund under contract number T026178.
♭ Supported also by the Comisión Interministerial de Ciencia y Tecnología.
♯ Also supported by CONICET and Universidad Nacional de La Plata, CC 67, 1900 La Plata, Argentina.
△ Supported by the National Natural Science Foundation of China.

$\sqrt{s}$ (GeV)	$\mathcal{L}$ (pb^{-1})	ϵ (%)	Back. (%)	Events	σ (pb)	σ_{SM} (pb)
188.6	172.1	28.9 ± 0.1	0.9	899	18.1 ± 0.6 ± 0.2	18.7 ± 0.2
191.6	17.9	28.2 ± 0.4	0.8	101	20.0 ± 2.1 ± 0.2	18.8 ± 0.2
195.5	74.9	27.1 ± 0.2	0.9	351	17.3 ± 1.1 ± 0.2	17.9 ± 0.2
199.5	67.4	27.3 ± 0.2	1.0	333	18.1 ± 1.0 ± 0.2	16.9 ± 0.2
201.7	36.5	27.4 ± 0.3	1.0	163	16.3 ± 1.3 ± 0.2	16.3 ± 0.2
202.5 − 205.5	78.7	25.0 ± 0.1	4.8	325	16.4 ± 1.0 ± 0.2	16.3 ± 0.2
205.5 − 207.2	124.1	25.2 ± 0.1	4.7	494	15.8 ± 0.7 ± 0.2	16.1 ± 0.2
207.2 − 209.2	8.2	24.8 ± 0.1	4.7	33	16.1 ± 3.0 ± 0.2	15.6 ± 0.2

Table 1: Integrated luminosities, $\mathcal{L}$, and results of the $e^+e^- \to q\bar{q}\gamma$ selection: selection efficiencies, ϵ, background level, number of selected events (background subtracted) and measured cross sections with statistical and systematic uncertainties. The uncertainty on ϵ comes from Monte Carlo statistics. The corresponding Standard Model cross sections, σ_{SM}, are listed in the last column. They are derived from the KK2f Monte Carlo generator [12]. Their uncertainty includes a 1% theory uncertainty and finite Monte Carlo statistics.

$\sqrt{s}$ (GeV)	$\mathcal{L}$ (pb^{-1})	ϵ (%)	Events	σ (pb)	σ_{SM} (pb)
188.6	175.6	32.3 ± 0.4	288	5.1 ± 0.3 ± 0.1	4.99 ± 0.05
191.6	16.9	31.4 ± 0.5	25	4.7 ± 0.8 ± 0.1	4.85 ± 0.05
195.5	80.9	31.5 ± 0.4	107	4.2 ± 0.4 ± 0.1	4.57 ± 0.05
199.5	79.5	28.0 ± 0.4	98	4.4 ± 0.4 ± 0.1	4.42 ± 0.05
201.7	36.1	30.8 ± 0.4	50	4.5 ± 0.6 ± 0.1	4.34 ± 0.04
202.5 − 205.5	74.3	28.9 ± 0.5	88	4.1 ± 0.4 ± 0.1	4.17 ± 0.04
205.5 − 209.2	129.6	29.4 ± 0.5	160	4.2 ± 0.3 ± 0.1	4.09 ± 0.04

Table 2: Integrated luminosities, $\mathcal{L}$, and results of the $e^+e^- \to \nu\bar{\nu}\gamma$ selection: selection efficiencies, ϵ, number of selected events and measured cross sections with statistical and systematic uncertainties. The uncertainty on ϵ comes from Monte Carlo statistics. The corresponding Standard Model cross sections, σ_{SM}, are listed in the last column. They are derived from the KKMC Monte Carlo generator [12]. Their uncertainty includes a 1% theory uncertainty and a contribution from finite Monte Carlo statistics.

	m_{rec} [GeV]				
$\lvert\cos\theta_\gamma\rvert$	$80-88$	$88-92$	$92-96$	$96-104$	$104-110$
$0.00-0.20$	14/20.4/0.0/78	64/ 69.8/ 0.0/35	79/ 62.3/ 0.0/35	58/ 55.8/ 0.5/57	43/24.0/0.3/67
$0.20-0.40$	19/27.1/0.0/85	91/ 86.4/ 0.0/37	92/ 75.4/ 0.9/38	62/ 68.2/ 0.3/62	31/26.9/0.7/64
$0.40-0.60$	26/25.7/0.0/62	116/110.1/ 0.4/37	121/107.9/ 0.5/41	79/ 83.8/ 0.6/64	35/32.9/0.6/64
$0.60-0.80$	29/19.3/0.2/28	88/ 84.1/ 0.5/17	75/100.6/ 0.1/24	82/ 92.3/ 1.3/43	37/40.7/0.5/48
$0.80-0.90$	35/39.7/0.6/61	145/167.4/ 0.4/35	127/159.6/ 1.9/40	161/136.1/ 4.3/63	68/55.7/1.9/70
$0.90-0.99$	95/55.9/4.6/18	302/276.8/11.5/12	271/281.9/11.8/15	232/225.8/12.3/24	98/87.1/4.4/24

Table 3: Numbers of events selected in the $e^+e^- \to q\bar{q}\gamma$ channel, Standard Model expectations, background level and selection efficiencies (in %) as a function of the recoil mass, m_{rec} to the photon candidate and of the absolute value of the cosine of the photon polar angle, $|\cos\theta_\gamma|$.

Source	Uncertainty (%)	
	$e^+e^- \to q\bar{q}\gamma$	$e^+e^- \to \nu\bar{\nu}\gamma$
Selection Process	0.8	1.5
Photon energy scale	0.4	0.6
MC statistics	≤ 0.4	0.4
Luminosity	0.2	0.2
Trigger efficiency	–	0.3
Background level	0.3	–
Total	1.1	1.7

Table 4: Sources of systematic uncertainty in the $e^+e^- \to q\bar{q}\gamma$ and $e^+e^- \to \nu\bar{\nu}\gamma$ cross sections.

Parameter	Fitted value	Negative error (95% CL)	Positive error (95% CL)
h_1^Z	-0.007	0.146	0.148
h_2^Z	-0.006	0.080	0.085
h_3^Z	-0.036	0.184	0.148
h_4^Z	0.038	0.106	0.110
h_1^γ	-0.001	0.056	0.058
h_2^γ	-0.014	0.035	0.037
h_3^γ	-0.026	0.033	0.031
h_4^γ	0.020	0.024	0.022

Table 5: Fitted values and errors at 95 % CL on the individual anomalous couplings from one-dimensional fits. In each fit the other seven parameters are set to zero.

Parameter	Fitted value	Negative limits	Positive limits	Correlation coeficient
h_1^Z	-0.05	-0.38	0.30	0.89
h_2^Z	-0.03	-0.22	0.18	
h_3^Z	-0.00	-0.46	0.40	0.90
h_4^Z	0.04	-0.24	0.28	
h_1^γ	-0.04	-0.15	0.07	0.85
h_2^γ	-0.03	-0.09	0.04	
h_3^γ	0.03	-0.09	0.14	0.93
h_4^γ	0.04	-0.04	0.11	

Table 6: Limits at 95 % CL on pairs of anomalous couplings from two-dimensional fits. In each fit the other six parameters are set to zero.

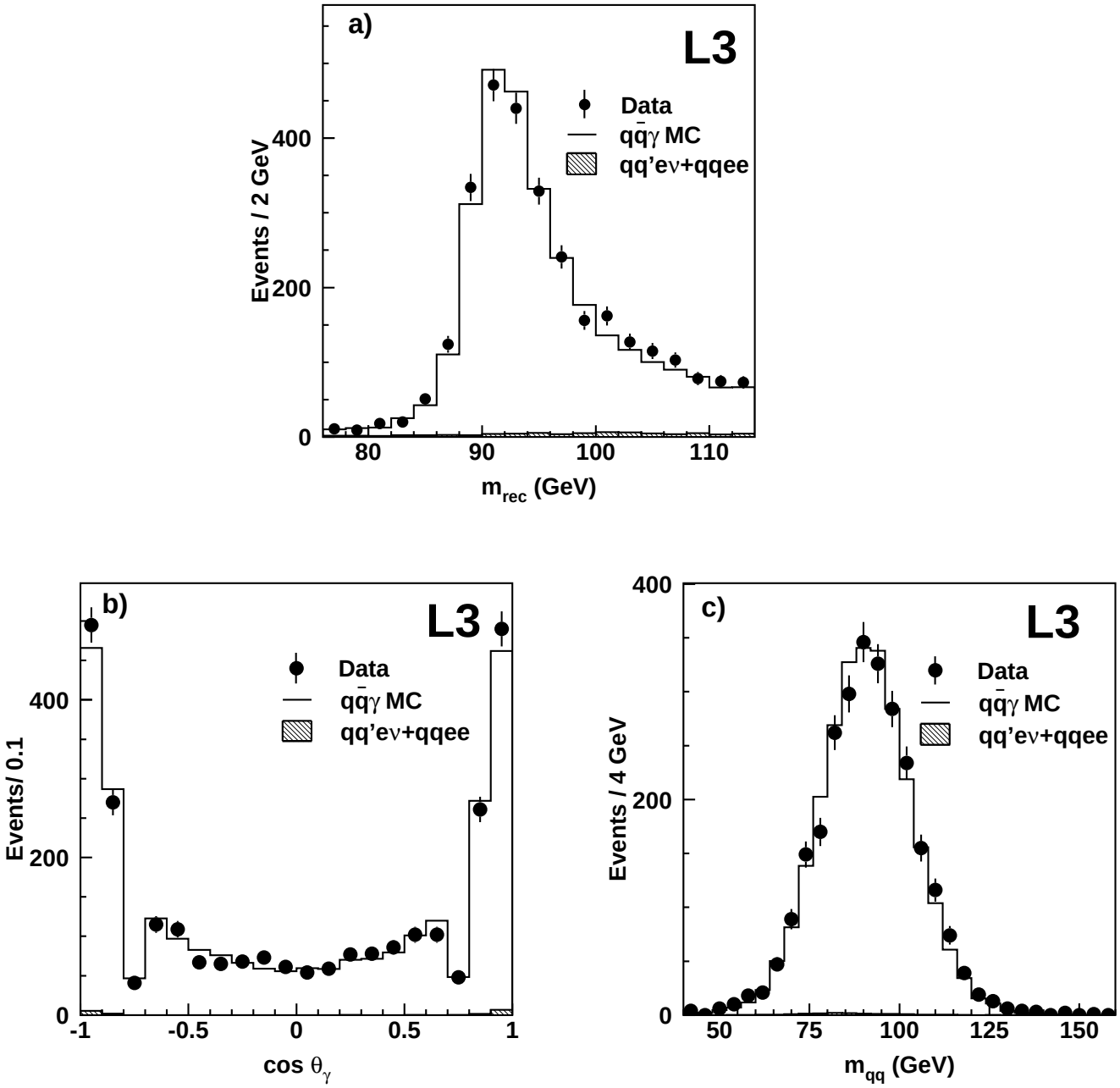


Figure 1: Distributions of a) the recoil mass to the photon candidate in $e^+e^- \to q\bar{q}\gamma$ events b) the polar angle of the photon and c) the invariant mass of the hadron system. The points are data, the open histogram is the Standard Model Monte Carlo prediction and the hatched one is the background from the $e^+e^- \to q\bar{q}'e\nu$ and $e^+e^- \to q\bar{q}e^+e^-$ processes.

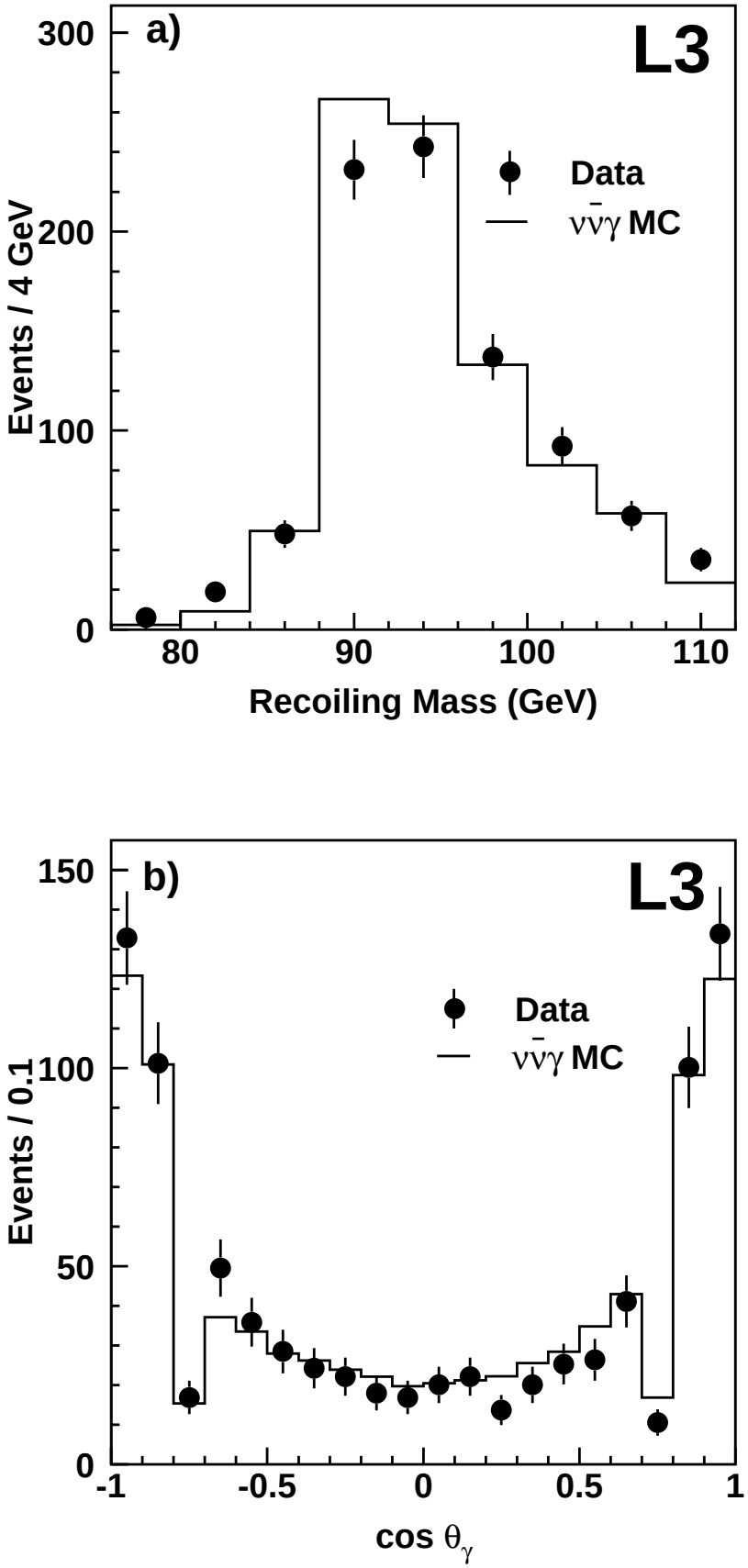


Figure 2: Distributions of a) the recoil mass to the photon candidate in $e^+e^- \to \nu\bar{\nu}\gamma$ events and b) the photon polar angle. The points are data and the histogram is the Standard Model Monte Carlo prediction.

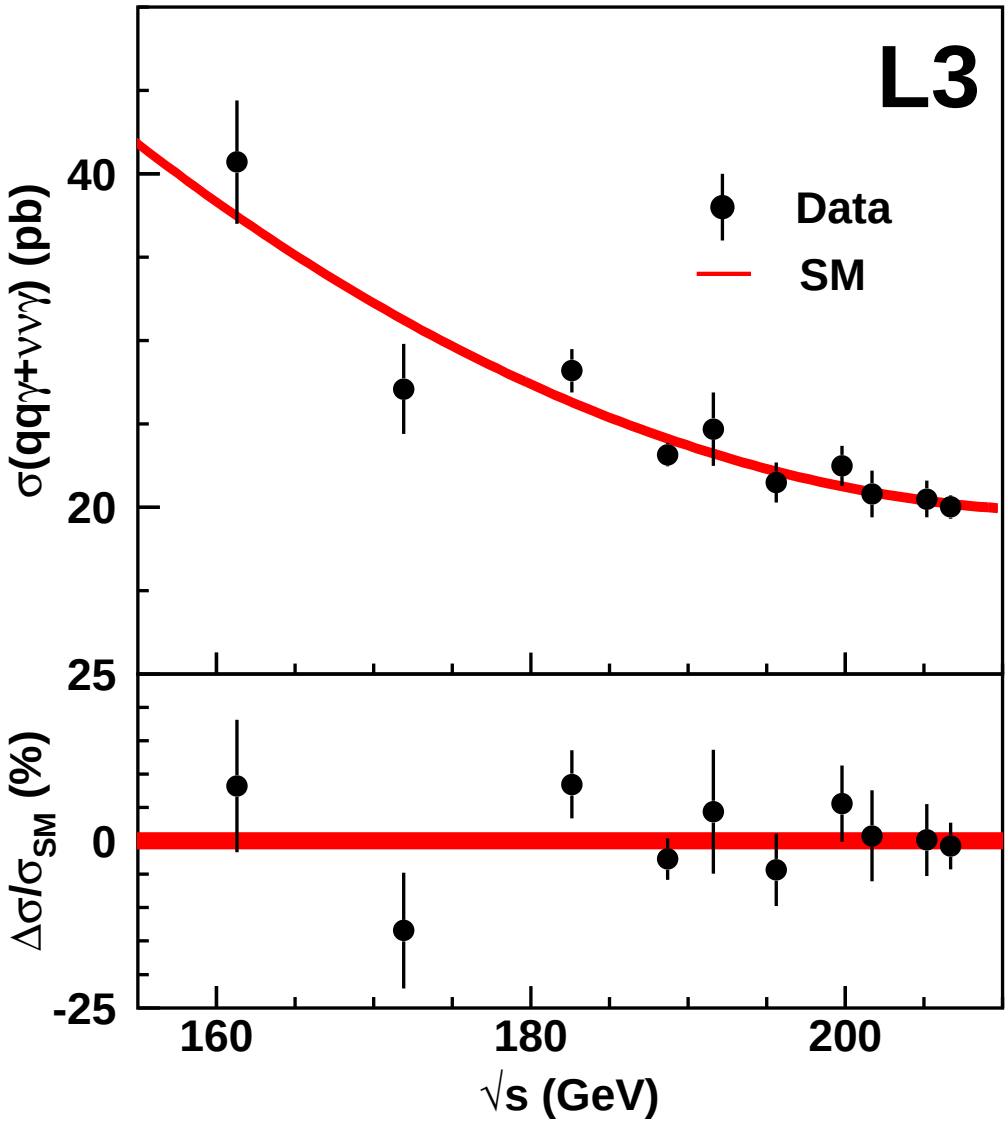


Figure 3: Variation of the sum of the cross-sections of the $e^+e^- \to q\bar{q}\gamma$ and $e^+e^- \to \nu\bar{\nu}\gamma$ processes, $\sigma(q\bar{q}\gamma + \nu\bar{\nu}\gamma)$, with $\sqrt{s}$. Data are represented by the dots, while the solid line gives the variation of the Standard Model cross-section, $\sigma_{\rm SM}$, as calculated with the KK2f and KKMC [12] Monte Carlo programs. The width of the band takes into account a 1% uncertainty in each of the $e^+e^- \to q\bar{q}\gamma$ and $e^+e^- \to \nu\bar{\nu}\gamma$ theoretical cross sections. The lower plot shows the relative difference.

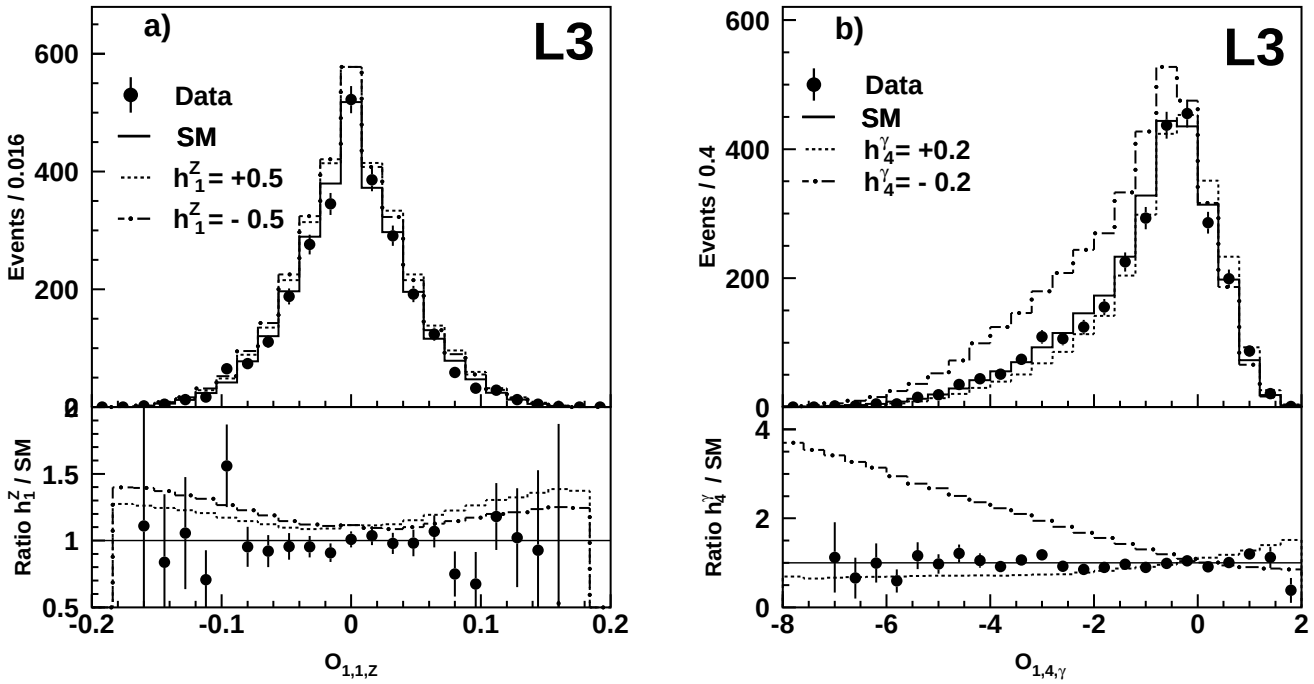


Figure 4: Distribution of the optimal variables for a) the CP-violating coupling h_1^Z and b) for the CP-conserving coupling h_4^γ. Data are shown together with the expectations for the Standard Model (SM) and for values of anomalous couplings $h_1^Z = \pm 0.5$ and $h_4^\gamma = \pm 0.2$. The lower plots shows the ratios between the anomalous coupling contributions and the data, to the Standard Model expectation.

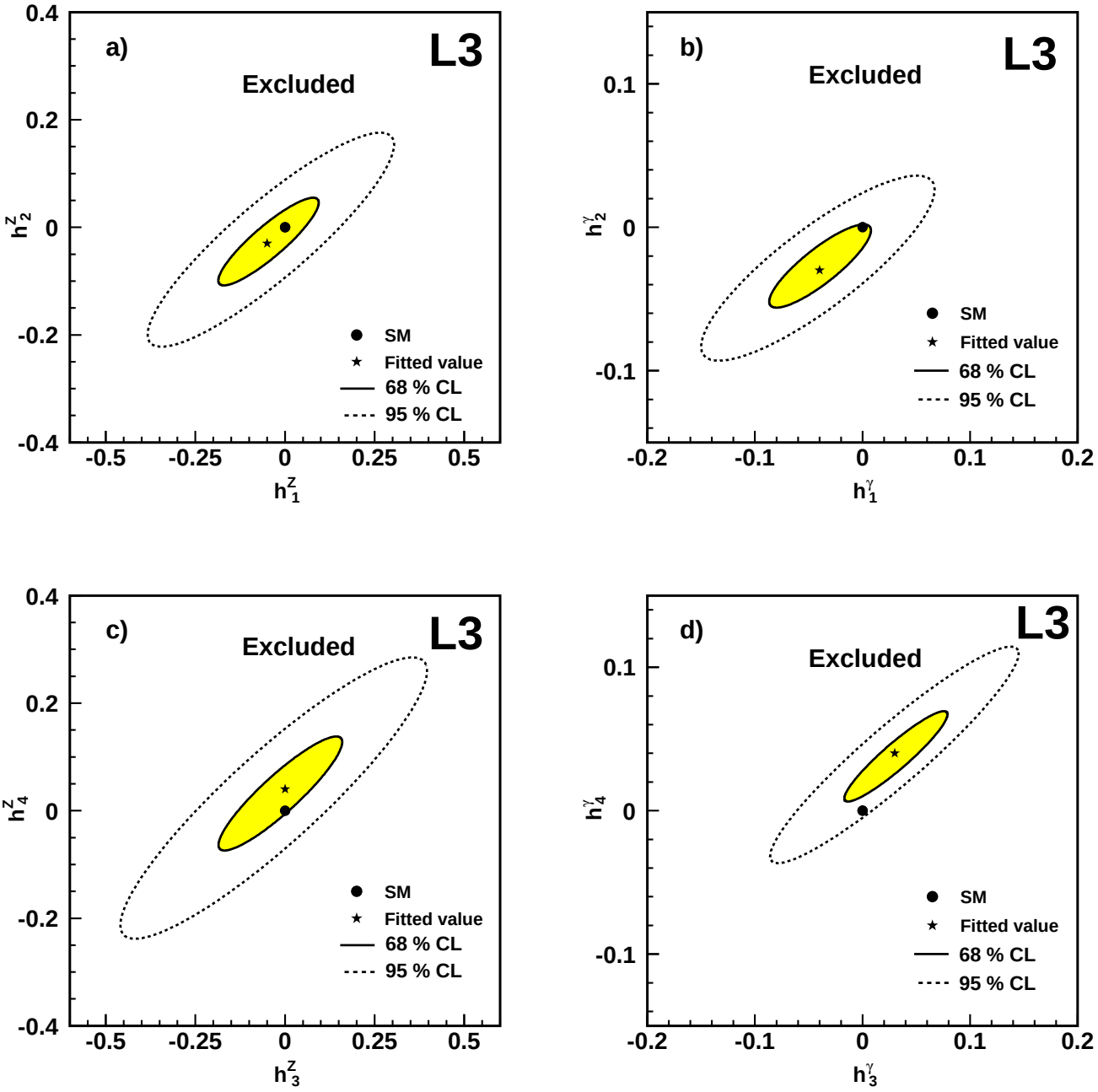


Figure 5: Two dimensional limits at 68% and 95% CL on the pairs of CP-violating coupling parameters, a) h_2^Z *vs.* h_1^Z and b) h_2^γ *vs.* h_1^γ and the pairs of CP-conserving coupling parameters, c) h_4^Z *vs.* h_3^Z and d) h_4^γ *vs.* h_3^γ. The Standard Model predictions are indicated by the points. The shaded areas correspond to the regions allowed at 68% CL while the dashed line shows the 95% CL exclusion contour.